Summer 5-12-2025

Observational Properties of Near-Maximal Spin Black Holes with the EHT

Tegan A. Thomas
Washington University in St. Louis

Angelo Ricarte
Black Hole Initiative

Yajie Yuan
Washington University in St. Louis

Recommended Citation

Observational Properties of Near-Maximal Spin Black Holes with the EHT

Tegan A. Thomas[1,2,3*] (iD)
Advisors: Angelo Ricarte[4,5] & Yajie Yuan[1]

[1]Department of Physics, Washington University in St. Louis, 1 Brookings Dr., St. Louis, MO 63130

[2]Smithsonian Astrophysical Observatory, 60 Garden St., Cambridge, MA 02138

[3]National Society of Black Physicists, 2010 Massachusetts Ave, Washington D.C., 20036

[4]Black Hole Initiative, Harvard University, 20 Garden St., Cambridge, MA 02138

[5]Center for Astrophysics, Harvard University & Smithsonian, 60 Garden St., Cambridge, MA 02138

ABSTRACT

In 2021 and 2024, the Event Horizon Telescope (EHT) collaboration published the first polarized images of the supermassive black holes (SMBHs) M87* and Sgr A*, which allowed us to place important constraints on the accretion flow and underlying space-time. Of particular interest is the dimensionless spin parameter "$a_\bullet$", which theoretically may attain a maximum value of $a_\bullet = 0.998$ when spun up by a thin accretion disk. On the other hand, mechanisms including incoherent accretion, SMBH mergers, and spin extraction via jets, are hypothesized to spin down SMBHs from these near-extremal values. In this work, we perform general relativistic magnetohydrodynamics (GRMHD) simulations of $a_\bullet = 0.998$ SMBHs with advection-dominated and strongly magnetized accretion disks to determine their observational characteristics. First, we evolve the fluid in a Kerr space-time to study black hole properties, including variability, magnetic flux accumulated on the horizon, and jet power. Then, we perform general relativistic ray-tracing (GRRT) to produce polarized movies that can be directly compared to current and future EHT observations. We predict increased jet power efficiency as well as distortions to the photon ring which should be an accessible signature that extensions to the EHT, such as the next-generation EHT (ngEHT) and Black Hole Explorer (BHEX), can then use to rule out such models.

1. INTRODUCTION

In 2019 the Event Horizon Telescope (EHT) collaboration successfully created the first image of a black hole with the picture of M87* (Event Horizon Telescope Collaboration et al., 2019a). This was then followed up with the image of the black hole at the center of the Milky Way, Sgr A* in 2022 (Event Horizon Telescope Collaboration et al., 2022a). These images have allowed us to gain incredible insight into the physics happening around supermassive black holes (SMBHs), as it serves as a source of data which may be compared against black hole models. The corresponding EHT polarized observation of M87* in 2021 and Sgr A* in 2024 helped map out the polarization structure of these sources, enhancing our models of near-horizon magnetic fields– a key probe of black hole spin (Event Horizon Telescope Collaboration et al., 2024a, 2021).

Moving forward, the next-generation Event Horizon Telescope (ngEHT) will improve upon the EHT by adding more radio dishes to the Very Long Baseline Interferometric (VLBI) array and observing at 3 frequencies simultaneously (Johnson et al., 2023). This will result in better resolution and spatial frequency coverage for observations of M87* and Sgr A* (Johnson et al., 2023). Additionally, the proposed Black

Hole Explorer (BHEX) mission would further expand the EHT into space, vastly improving our resolution to the order of 5μas (Johnson et al., 2024). With BHEX, additional sources besides Sgr A* and M87* will become observationally accessible, further increasing the importance of having methods with which we may constrain black hole parameters such as inclination or magnetic field strength (Johnson et al., 2024).

One of the key parameters in this context is the dimensionless spin parameter $a_\bullet$, as defined by the equation below where J is the angular momentum and $M_\bullet$ is the black hole mass (Event Horizon Telescope Collaboration et al., 2019b). Especially when looking at event horizon scale observations, $a_\bullet$ is critical as it significantly impacts evolution and dynamics of the nearby disk.

$$a_\bullet = \frac{cJ}{GM_\bullet^2} \tag{1}$$

$a_\bullet$ is measured between -1 and 1, however due to radiation the upper limit of a black hole's spin is 0.998 for black holes with a thin accretion disk (Thorne, 1974). Despite this, it has been shown that black holes do not always reach this maximum spin of 0.998 and can instead reach equilibrium at lower spins (Gammie et al., 2004; Shapiro, 2005; Narayan et al., 2022; Ricarte et al., 2023a; Lowell et al., 2024, 2025).

In addition to impacting the dynamics of the accretion disk, spin also has cosmological importance. For instance, the spin distribution of black holes in the universe can indicate if accretion flows are typically coherent over cosmological timescales (Berti and Volonteri, 2008) and the role that angular momentum loss due to jets may play in spin evolution (Ricarte et al., 2023a). Multiple proposed methods of spin evolution have even found that, theoretically, there should be nearly no maximally spinning black holes (Berti and Volonteri, 2008; Ricarte et al., 2025). Therefore observing a maximally spinning black hole, or being able to rule out a significant number of black holes as not maximally spinning, would help narrow our options for spin evolution mechanisms and would have significant cosmological implications.

In order to observe such an object, we must first know what near-maximal spin SMBHs should look like. As spin approaches 1, many black hole properties evolve rapidly, potentially resulting in unique observational signatures. Our project aims to identify observational characteristics of near-maximal spin black holes and probe evolution over spin by presenting one of the first polarized movies of a simulated $a_\bullet = 0.998$ SMBH and comparing it to a $a_\bullet = 0.9375$ counterpart.

In section 2 we review foundational black hole theory as it relates to this project. Section 3 focuses on the code used, specifically KHARMA for GRMHD and IPOLE for GRRT. Additionally, we will explain the units used and potential limitations to the simulations. In section 4 we present and analyze our preliminary results before going to section 5 where we discuss the implications for potential EHT observations of maximally spinning black holes.

2. THEORY OF KERR BLACK HOLES AND THEIR OBSERVABLES

2.1. Jet Luminosity

The Blandford-Znajek mechanism is a key model that links relativistic jet power to black hole spin (Blandford and Znajek, 1977).

The model suggests that, due to the spin of BH, the magnetic field which threads the black hole is twisted into coils, forming a large toroidal field component along the jet. This toroidal field then exerts an upward magnetic pressure on the surrounding plasma which builds over time. Eventually, in order to

maintain stability, the plasma pressure must decrease by accelerating plasma upwards, creating a jet (Davis and Tchekhovskoy, 2020; Blandford and Znajek, 1977).

This process is best demonstrated with the diagram below (Davis and Tchekhovskoy, 2020).
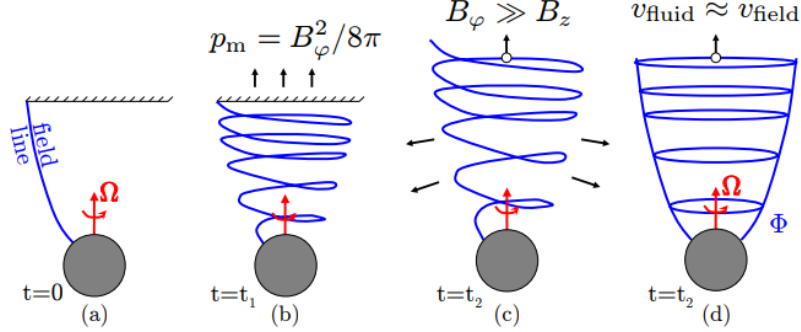
Figure 1. Above is a diagram from Davis & Tchekhovskoy (2021) demonstrating the BZ mechanism (Davis and Tchekhovskoy, 2020). As a black hole spins it twists the initially poloidal magnetic fields, producing a toroidal component. This component builds up, becoming a "magnetic spring" of sorts and eventually it is large enough to push away a layer of plasma and it begins to continually accelerate plasma upwards. Eventually the magnetic field can be estimated as primarily toroidal, at which point the plasma acceleration is mainly driven by the established pressure gradient.

Since the jet is driven by the dragging of the magnetic fields it makes sense that, for slowly spinning black holes ($a_\bullet << 1$), the jet luminosity relates to magnetic flux onto the horizon (Φ_B) and spin ($a_\bullet$) via the equation below.

$$L_{BZ} \propto a_\bullet^2 \Phi_B^2 \tag{2}$$

As the spin approaches one, the jet becomes more luminous and powerful, extracting increased amount of energy from the black hole. This is evaluated using the jet power efficiency, defined below.

$$\eta = \frac{P_{jet}}{\langle \dot{M}_0 \rangle c^2} \tag{3}$$

In this paper, "accretion rate", $\dot{M}_0$, specifically refers to the rest mass inflow rate through the disk, not necessarily the net rate of change of the black hole rest mass (Ricarte et al., 2025).

For black holes with sufficiently large magnetic fields, known as MADs, Narayan et al. (2022) finds that this jet power efficiency increases with increased spin in such a way that agrees with the predicted relationship found in Tchekhovskoy et al. (2010) written below.

$$\eta_{BZ6} = \frac{\kappa}{4\pi} \phi_{BH}^2 \Omega_H^2 [1 + 1.38\Omega_H^2 - 9.2\Omega_H^4] \tag{4}$$

where $\Omega_H = \frac{a_\bullet}{2r_H}$. Specifically, Narayan et al. (2022) found agreement between their findings and Tchekovskoy's equation for $\kappa = 0.05$, where κ is a constant whose precise value is determined by the initial field geometry. It is expected that, for the near-maximal spin case, this jet power efficiency should continue to increase even beyond 1, implying that more energy is extracted via the jet than produced from accretion. Such behavior was observed for MAD models with a spin of 0.9, but should be more extreme for the near-maximal spin of 0.998.

For MAD systems, the angular momentum and energy loss from these powerful jets may exceed the momentum gained from the disk, resulting in the black hole spinning down (Narayan et al., 2022). The spin-up of a black hole is analyzed using the dimensionless spin up parameter *s* as defined below where a

negative value indicates spin down ([Gammie et al., 2004](); [Shapiro, 2005](); [Ricarte et al., 2025]()).

$$s = \frac{d(J/M^2)}{dt}\frac{M_\bullet}{\dot{M}_0} = \frac{da_\bullet}{dt}\frac{M_\bullet}{\dot{M}_0} \tag{5}$$

As the spin increases, this spin up parameter should become increasingly negative indicating intense spin down of the black hole ([Narayan et al., 2022]()). In this way, jets heavily influence the spin evolution of black holes.

Jet power is also important because of the role jets play in galaxy evolution. Jets insert large amounts of energy within their host galaxies over very long distances which heats galaxy halos and prevents gas from cooling, potentially limiting star formation. The heated gas also is more broadly distributed and less dense, resulting in decreased accretion and therefore decreased jet power. This cycle of influence between jets and their host galaxies is known as jet-driven AGN feedback and is a blossoming area of research as the exact mechanisms and impacts of large jet power are still being determined.

It is through AGN feedback as well as BH spin evolution that our findings on jet power efficiency for near-maximal black holes can have important implications about galaxy evolution as a whole.

2.2. Accretion Flow Properties

Besides the impact on jets, the spin of a black hole also directly determines the position of the event horizon, which in turn also influences accretion flow.

The event horizon is defined as the surface beyond which there do not exist outgoing geodesics. The equation for the event horizon radius is below.

$$r_{EH} = \frac{GM_\bullet}{c^2}\left[1 + \sqrt{1 - a_\bullet^2}\right] \tag{6}$$

As spin increases, the event horizon shrinks causing a number of important effects. In particular, the event horizon shrinking has been shown to result in increased accretion disk temperature, which is expected due to the conversion of a greater amount of gravitational potential energy into heat as the horizon shrinks ([Event Horizon Telescope Collaboration et al., 2022b]()).

In addition, the spin of a black hole directly influences the magnetic field morphology within the accretion disk. Specifically, as a black hole's spin increases, frame dragging effects become more intense, resulting in more toroidal magnetic fields ([Ricarte et al., 2022]()). While General Relativity provides us with an analytical framework to evaluate frame dragging at arbitrary spin values, GRMHD and GRRT models aimed at understanding the observational implications haven't been well studied for spin values above $a_\bullet = 0.9375$.

2.3. Ray Tracing

The Event Horizon Telescope is able to image black holes on event horizon scales because not all of the emission from the accretion disk around a black hole falls into the black hole. Instead, some of the light is lensed by the black hole's intense gravity and eventually makes its way to Earth, which is what the EHT observes.

Out of this light that is eventually observed, most of it was emitted and directly lensed in our direction. However, the gravitational lensing of the black hole is powerful enough that some photons orbit the black hole before going in our direction, creating a fainter ring of light within our final image which we call the photon ring.

Within the photon ring there are sub-rings that are indexed by n, where each photon within that sub-ring has performed [n+1,n+2) half-orbits (Palumbo et al., 2023). As $n \rightarrow \infty$ the image approaches the "critical curve"; an image predicted by General Relativity that acts as the boundary between the geodesics that can and can't reach us (Palumbo et al., 2023). This critical curve can be analytically determined by the mass, distance, spin, and viewing inclination of the black hole (Palumbo et al., 2023).

Given that, for most black hole sources potentially resolvable to the EHT, the mass and distance can be approximated using other astronomical methods or the general size of the black hole shadow, being able to resolve the critical curve would give us key information to constrain the potential combinations of spin and inclination.

The n=0 ring dominates most emission, and each subsequent ring gets substantially fainter as the parameters that allow for multiple orbits become more constrained. This exponential drop-off in intensity makes imaging the critical curve directly nearly impossible. However, the rings also approach the shape of the critical curve exponentially, meaning that even with small values of n we can infer what the critical curve may look like. This makes the n=1 photon ring in particular very promising as it is the most feasible of the rings (aside from n=0) to resolve, but it also still provides significant insight into the potential spin and inclination of a black hole. Efforts are being made to resolve the photon ring of M87* or Sgr A* using the ngEHT and the Black Hole Explorer (BHEX) in the future (Johnson et al., 2024).

Looking at spin specifically, the critical curve changes in diameter, position, and shape as spin increases. These changes are also dependent on the inclination and typically edge-on inclination allows for the most noticeable photon ring differences as demonstrated below.
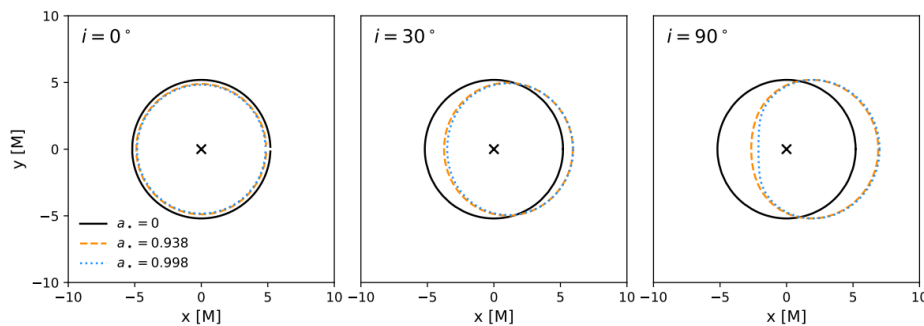
Figure 2. The analytically determined critical curve for spins of $a_\bullet = 0, 0.9375$, and 0.998 is shown for inclinations of $0°$, 30 °, and 90 °. The code to make this image is from Ricarte et al. 2023 (Ricarte et al., 2023b), and is based on equations from Chael et al. 2021 (Chael et al., 2021).

The figure demonstrates how, at 0°inclination, the primary effect is on the decreasing radius of the critical curve for increasing spin, meanwhile for 30°, a translational shift becomes noticeable, and at 90°the shape of the curve is impacted as it flattens on the left-hand side with increasing spin.

Aside from the photon ring, spin significantly influences photon geodesics and ray tracing because of its effects on the event horizon. As mentioned before, the event horizon shrinks with increasing spin, allowing us to probe the area closer to the black hole. While the emission from nearby the event horizon is significantly redshifted, it still constitutes a notable portion of our observed emission which is known as the "inner shadow" (Chael et al., 2022). This inner shadow appears as a brightness depression, the edge of which is a lensed image of the event horizon (Chael et al., 2022). Being able to observe and identify such a feature would not only directly allow us to probe black hole spin, since the event horizon radius is directly related to spin, but

also would help indicate accretion disk & jet geometry as the inner shadow only appears in the case that emission is concentrated to the equatorial plane (Chael et al., 2022).

3. METHODOLOGY

3.1. GRMHD Simulations

For our GRMHD simulations, we followed the framework outlined in Wong et al. (2022).

In order to model the plasma around black holes we use the General Relativistic Magneto-Hydrodynamic (GRMHD) code known as KHARMA. KHARMA works by utilizing Parthenon to track the density (ρ), internal energy (u), four-velocity ($\tilde{u}^i$), and magnetic field (B^i) of the plasma as it travels between cells (Wong et al., 2022). These are known as our "primitive variables" and they are used to compute conserved quantities such as the stress energy tensor T^μ_ν (Wong et al., 2022). The equations which govern GRMHD and allow us to calculate conserved quantities from primitive variables are listed below.

$$\delta_t(\sqrt{-g}\rho u^t) = -\delta_i(\sqrt{-g}\rho u^i) \tag{7}$$

$$\delta_t(\sqrt{-g}T^t_\nu) = -\delta_i(\sqrt{-g}T^i_\nu) + \sqrt{-g}T^\kappa_\lambda\Gamma^\lambda_{\nu\kappa} \tag{8}$$

$$\delta_t(\sqrt{-g}B^i) = -\delta_j[\sqrt{-g}(b^j u^i - b^i u^j)] \tag{9}$$

$$\delta_i(\sqrt{-g}B^i) = 0 \tag{10}$$

In these equations g is the determinant of the Kerr metric and Γ is the Christoffel symbol.

3.1.1. Units

Throughout this paper, distance and time is expressed in terms of M, the black hole mass parameter $GM_\bullet/c^2$, based on the following equations for gravitation radii and time.

$$\begin{aligned} r_g &= \frac{GM_\bullet}{c^2} \\ t_g &= \frac{GM_\bullet}{c^3} \end{aligned} \tag{11}$$

Additionally, within KHARMA we utilize a coordinate system known as "Modified Kerr-Schild" or mks. mks establishes a grid, demonstrated below, with increasing density around the midplane based on a parameter known as hslope, which we choose to be 0.3.
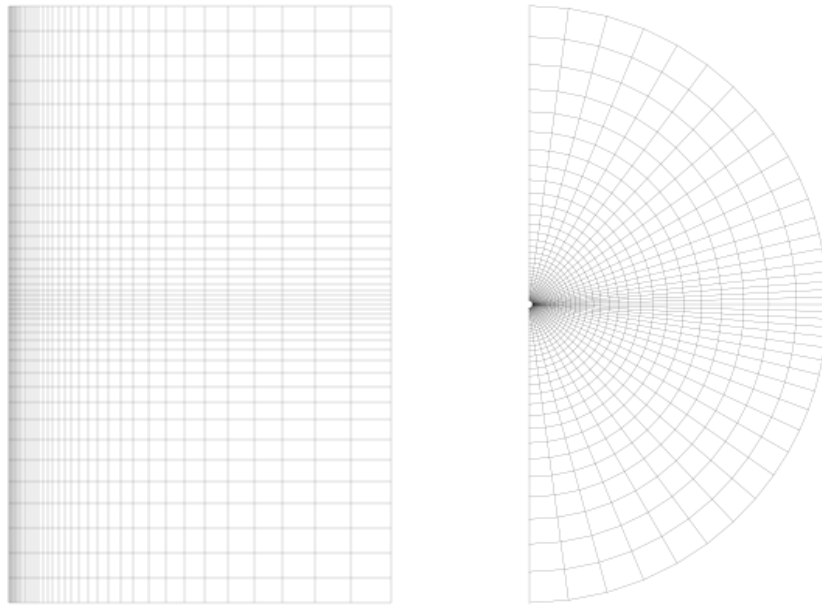
Figure 3. On the left is a demonstration of mks coordinates on a (r,θ) plot where radius increases along the x-axis and θ along the y-axis. On the right is a demonstration of mks coordinates within a polar plot. As mks coordinates are spherical in nature, this polar plot better reflects a ZX slice of a KHARMA simulation.

The rectangles defined by the radial and θ curves are known as "grid zones" and within each zone the primitive variables are stored, effectively simulating a block of plasma within that region. Neighboring zones impact one another, simulating the fluid's movement, and the magnetic field is calculated along the face of each grid zone which also impacts the plasma dynamics appropriately. Resolution within GRMHD refers to how many of those grid zones are present in each direction and our simulations use a resolution of 288x128x128.

When defining the grid, in order to ensure efficient runtime one must choose the inner and outer radial boundaries at which the grid should start and end. The outer radial boundary is taken such that the torus and accretion disk can always fully fit within the grid. The inner radial boundary is taken such that we always have at least 5 zones placed within the event horizon. This is done in order to ensure that material falling into the event horizon still behaves in a physical manner and doesn't cause any unexpected behavior that may impact your measurements.

3.1.2. Initial Conditions & Parameters

We begin each simulation with a Fishbone & Moncrief torus with an innermost radius of $r_{in} = 20r_g$ and a radius of maximum pressure of $r_{max} = 41r_g$ centered around the black hole (Fishbone and Moncrief, 1976). We establish the black hole as having some spin $a_\bullet$ and apply MAD magnetic field initial conditions to the torus. From there, due to the magnetic field, the plasma begins accreting over time. We primarily focus on the results from the simulation past $t \approx 5,000t_g$ as beyond that point the black hole should be relatively stable and should no longer be significantly impacted by the initial torus condition.

Throughout the simulation we maintain a constant adiabatic index $\hat{\gamma}$ of $\frac{13}{9}$, which is between the expected

index values of $\frac{5}{3}$ and $\frac{4}{3}$ for plasma temperatures below and above $\frac{m_e c^2}{k_b}$ respectively (Mignone and McKinney, 2007).

For these runs we focus on Magnetically Arrested Disks (MAD) where the magnetic flux upon the horizon builds via constant accretion until it becomes sufficiently large and dynamically important as the magnetic pressure counteracts the inflow (Narayan et al., 2003). In comparison, Standard and Normal Evolution (SANE) disks have a weak turbulent magnetic field which does not become dynamically important and doesn't magnetically arrest the fluid despite simulating over long time frames (Narayan et al., 2012). MAD models are currently preferred in most cases based on EHT observations of Sgr A*, which is why we utilize them in this work (Event Horizon Telescope Collaboration et al., 2022b). Future work may include performing a similar study with SANE models instead.

The near-maximal spin KHARMA run faced some difficulties with floors resulting in material being inserted along the jet, and so transmitting boundary conditions and B_ϕ reconnection was adopted. These changes make it so that magnetic loops around the pole can be connected despite being in different grid zones, preventing $\nabla \cdot B$ from growing uncontrollably, and also allow for inserted material to better distribute along the poles, preventing a large amount of material inserted on one side from building up and causing an explosion.
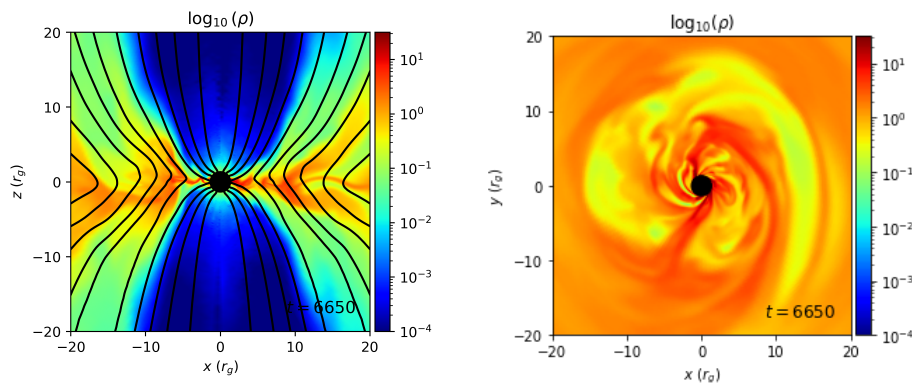
Figure 4. Above are two images showing the xz and xy slice of a typical GRMHD snapshot. The color denotes the log density and the contour lines show the poloidal magnetic field.

3.2. GRRT Imaging

In order to image the GRMHD simulations we get from KHARMA we utilize the General Relativistic Radiative Transfer (GRRT) code known as IPOLE , which is explained in more detail in Mościbrodzka and Gammie (2018). IPOLE works by first establishing a grid and information about the black hole and plasma using files from KHARMA. It then tracks the photon path from the camera towards the black hole, stopping once it hits the event horizon, goes off past a certain radius, or once a maximum number of steps has been taken. Finally, it integrates the equations of polarized radiative transfer forward towards the camera. Throughout these steps we have taken on the "fast-light" assumption which argues that the timescale it would take for the light to travel through the accretion disk is small enough that the disk doesn't change during it, and so we create a single image from a single GRMHD file. The radiative transfer equations can be found

below.

$$\frac{d}{ds}\begin{pmatrix} I_\nu \\ Q_\nu \\ U_\nu \\ V_\nu \end{pmatrix} = \begin{pmatrix} j_{\nu,I} \\ j_{\nu,Q} \\ j_{\nu,U} \\ j_{\nu,V} \end{pmatrix} - \begin{pmatrix} \alpha_{\nu,I} & \alpha_{\nu,Q} & \alpha_{\nu,U} & \alpha_{\nu,V} \\ \alpha_{\nu,Q} & \alpha_{\nu,I} & \rho_{\nu,V} & -\rho_{\nu,U} \\ \alpha_{\nu,U} & -\rho_{\nu,V} & \alpha_{\nu,I} & \rho_{\nu,Q} \\ \alpha_{\nu,V} & \rho_{\nu,U} & -\rho_{\nu,Q} & \alpha_{\nu,I} \end{pmatrix}\begin{pmatrix} I_\nu \\ Q_\nu \\ U_\nu \\ V_\nu \end{pmatrix} \qquad (12)$$

In this equation, I Q U & V are the Stokes parameters indicating overall intensity (I), linear polarization intensity (Q and U), and circular polarization intensity (V). The values $j_{\nu,\_}$, where _ represents one of the four Stokes parameters, represent the emission coefficients, the values $\alpha_{\nu,\_}$ represent the absorption coefficients, and the values $\rho_{\nu,\_}$ represent the rotation coefficients. In this way, the equation shows that the change in intensities over each step is based on the amount of new emission minus the amount of absorption and rotation that acts on previous emission. Since we track of all of the Stokes parameters, IPOLE produces fully polarized images. Only synchrotron radiation is considered as it dominates current EHT observations, although bremmstrahlung and inverse Compton scattering are believed to become more important in the near infrared and higher frequencies. For this work all images are taken at 230GHz, although in the future it may be worthwhile to investigate observational signatures in other frequencies.

With IPOLE we are able to image GRMHD simulations at arbirarily high resolution, which allows for us to explore theoretical effects of certain characteristics on images. However, in order to properly compare with EHT data we apply a Gaussian beam to blur the image so that it is comparable to EHT's resolution of $20\mu as$.
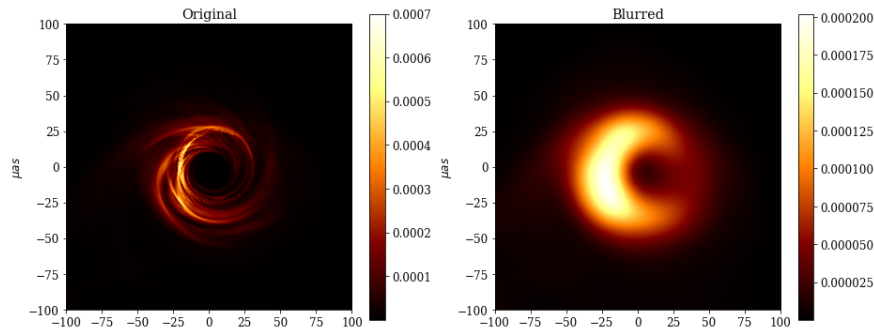
Figure 5. Above is an example of an IPOLE snapshot. On the left is the original image produced by IPOLE and then on the right is a blurred version which shows what EHT would actually observe.

Additionally, since we track the null geodesic that photons travel upon, we are able to easily decompose the photon rings, allowing us to analyze how they are impacted by maximal spin.

In order to produce a movie using IPOLE we simply image a series of GRMHD files chronologically and then use a software such as FFMPEG to produce a video. One caveat to this is that GRMHD uses M as its mass unit which is then used to scale most other measurements(including time and distances) and there is therefore some associated simulation mass density. In order to image though, we need some scaling factor $\mathcal{M}$ to convert the simulated mass density into physical units (Mościbrodzka and Gammie, 2018). In particular, it is required that we scale the simulated compact flux density to be in agreement with observational constraints (Mościbrodzka and Gammie, 2018). Within IPOLE, the variable "M_unit" serves this role as it is used to scale the accretion rate of the black hole to a known object's flux. In this case we match it to Sgr A*'s flux of $\approx 2.4Jy$. From there, the angular scale of the image produced by IPOLE is determined by M and the distance that the camera is placed at.

4. RESULTS

The aforementioned process was used to model and image black holes with $a_\bullet = 0.9375$ and $a_\bullet = 0.998$ and for inclinations of 150°and 90°. Our GRMHD simulations ran up till $10,000t_g$, although the first $5,000t_g$ timesteps aren't included in these results in order to avoid any influence of initial conditions. The following results and analysis are all based on the $5,000 - 10,000t_g$ time window for both simulations.

4.1. Black Hole Properties

4.1.1. Accretion Rate

The accretion rate is calculated within PYHARM by looking at the mass flux (rate of mass flow per unit area) at $5r_g \pm 0.05r_g$ (where the $\pm 0.05r_g$ is due to zone boundaries not aligning strictly at $5r_g$) and is represented with the variable $\dot{M}$.
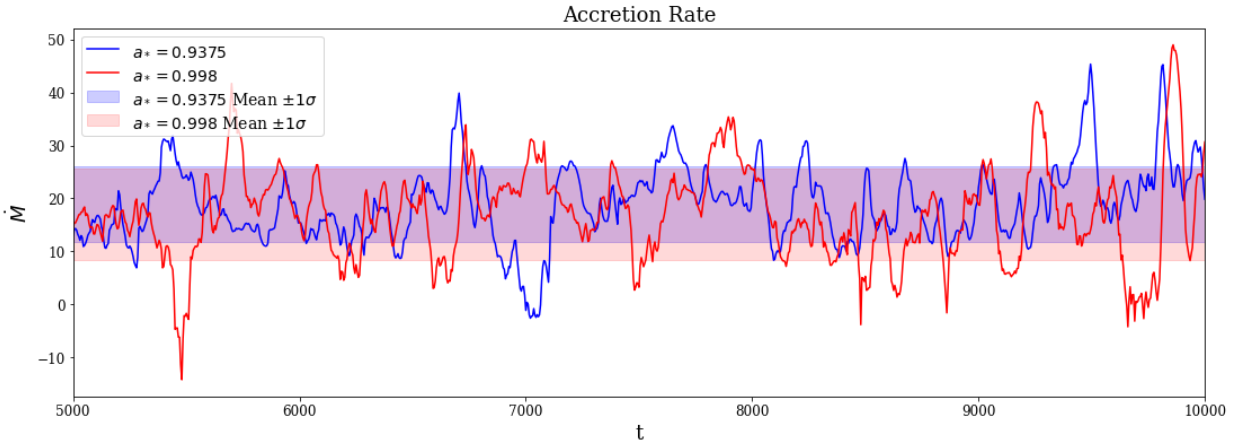
Figure 6. The accretion rate as a function of time is shown for both $a_\bullet = 0.9375$ (blue) and $a_\bullet = 0.998$ (red). The highlighted blue and red regions show the mean accretion rate $\pm 1\sigma$ for $a_\bullet = 0.9375$ and 0.998 respectively.

In code units, the average accretion rate for $a_\bullet = 0.9375$ versus $a_\bullet = 0.998$ is ~18.84 and ~16.97 respectively. While they are not significantly different, we do still note the decrease in accretion rate for the near-maximal case.

The $a_\bullet = 0.9375$ and $a_\bullet = 0.998$ simulations had a σ/μ of 0.378 and 0.512 respectively. This indicates that the near-maximal case has more variable accretion rate, which is important as that is expected to also produce higher total intensity variability. Currently, within the EHT collaboration, most models, including the 0.9375 models, overestimate the variability of Sgr A* when compared to observations (Event Horizon Telescope Collaboration et al., 2022b), and so the near-maximal case potentially having a larger variability than the $a_\bullet = 0.9375$ case indicates that it may not be as likely of a candidate for Sgr A*.

We note the prevalence of "flux eruption events" as well within both simulations. Flux eruption events are periods of time where there is a sharp decrease in accretion rate and physically they correspond to magnetic field reconnection releasing large amounts of magnetic energy into the plasma, pushing material in the disk away from the black hole. We see such events occur at $\approx 7,000t_g$ for $a_\bullet = 0.9375$ and at $\approx 9,700t_g$ and $\approx 5,400t_g$ for $a_\bullet = 0.998$.
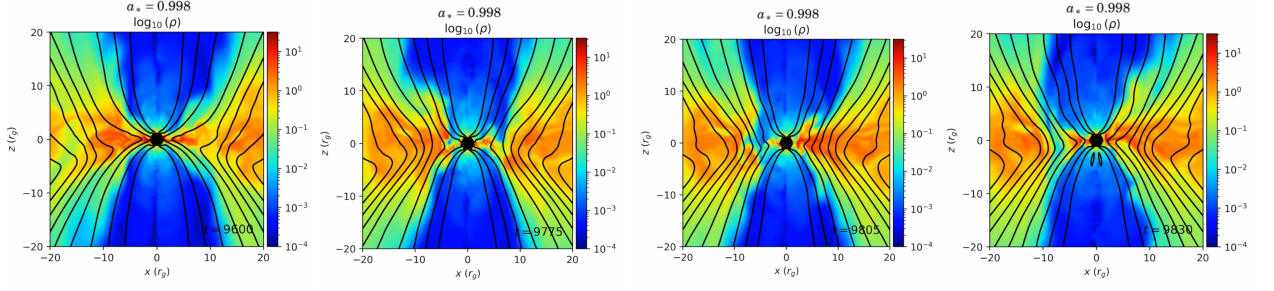
Figure 7. Density plots of the KHARMA GRMHD $a_\bullet = 0.998$ run during a flux eruption event which roughly follow local peaks in ϕ_{BH} taken at $9,600, 9,775, 9,805$, and $9,830 t_g$ from left to right.

4.1.2. Magnetic Field

4.1.2.1. Magnetization Within the MAD state, the plasma has some initial poloidal magnetic field and as that plasma accretes onto the black hole some of the magnetic field lines thread through the BH horizon, resulting in a net magnetic flux. This magnetic flux is most commonly measured via the dimensionless the magnetic flux parameter ϕ_{BH}, which is calculated using the equation below (Tchekhovskoy et al., 2011; Narayan et al., 2022).

$$\phi_{BH}(t) = \frac{\sqrt{4\pi}}{2\sqrt{\dot{M}_0(t)}} \int_\theta \int_\phi |B^r|_{r_H} \sqrt{-g} d\theta d\phi \tag{13}$$

The $\sqrt{4\pi}$ term converts the magnetic field strength B^r from Heaviside-Lorentz units to Gaussian units, $\dot{M}_0$ is the rest mass inflow rate through the disk as a function of time, g is the determinant of the metric, and r_H is the event horizon radius.

Using PyHARM, ϕ_{BH} is tracked as a function of time and magnetic flux is measured at $r_H \pm 0.01 r_g$ while accretion rate is measured at $5r_g \pm 0.05 r_g$. Previous studies of GRMHD simulations have suggested the following equation for ϕ_{BH} as a function of spin (Tchekhovskoy et al., 2012; Narayan et al., 2022).

$$\phi_{BH} = -20.2a_\bullet^3 - 14.9a_\bullet^2 + 34a_\bullet + 52.6 \tag{14}$$
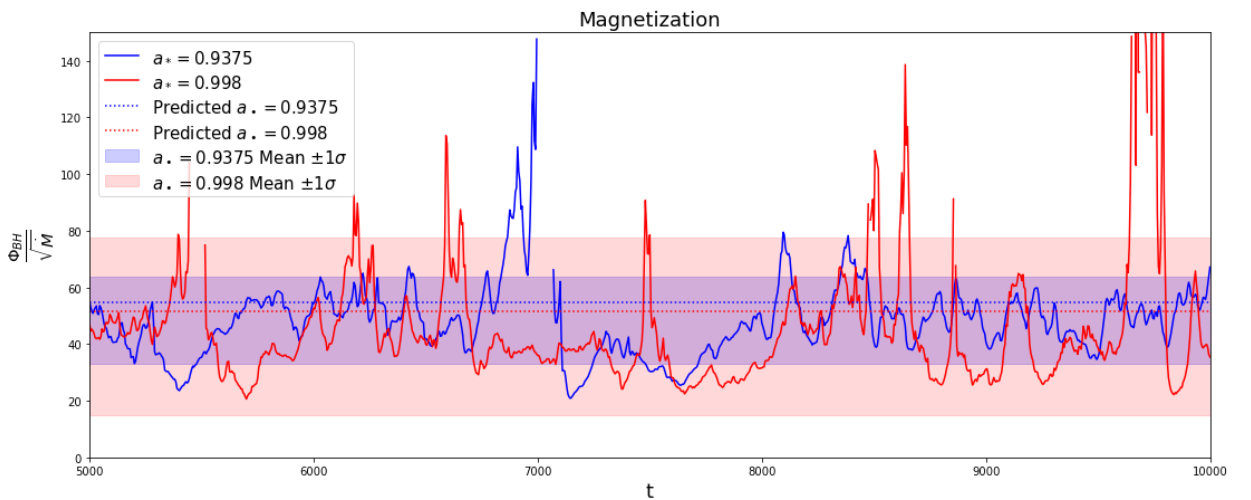
Figure 8. The magnetization as a function of time is shown for both $a_\bullet = 0.9375$ (blue) and $a_\bullet = 0.998$ (red). Additionally, the dashed horizontal lines reflect the predicted magnetization based on Tchekhovskoy et al. (2012) (Tchekhovskoy et al., 2012; Narayan et al., 2022). For $a_\bullet = 0.9375$ and $a_\bullet = 0.998$ these values are ~54.735 and ~51.612 respectively. The highlighted blue and red regions show the mean of magnetization $\pm 1\sigma$ for $a_\bullet = 0.9375$ and 0.998 respectively.

The average ϕ_{BH} for $a_{\bullet} = 0.9375$ versus $a_{\bullet} = 0.998$ is ~48.351 and ~46.094 respectively which differs from the predicted ~54.735 and ~51.612.

These predicted values being higher in both spin cases may be due to the fact that equation 14 was based on GRMHD simulations which used an adiabatic index $\hat{\gamma} = \frac{5}{3}$ (Tchekhovskoy et al., 2012; Narayan et al., 2022). Our lower $\hat{\gamma}$ of $\frac{13}{9}$ then may contribute to the lower than expected magnetization values.

That being said, our simulations do confirm that ϕ_{BH} decreases with increasing spin.

Additionally, the near-maximal case demonstrates considerably larger variability, with σ/μ values of 0.679 for the $a_{\bullet} = 0.998$ case and 0.317 for the $a_{\bullet} = 0.9375$ case. Much of this variability appears to be due to the large magnetization preceeding the flux eruption event at $\approx 9,7000 t_g$, which is demonstrated in figure 7.

Many of the peaks in magnetization for the $a_{\bullet} = 0.998$ case align with quasi-periodic dips in accretion rate of varying intensities, the most intense of which are flux eruption events. This potentially suggests that for near-maximal spin it may take a slightly longer time for the black hole to reach an equilibrium between the inward pressure from the accreting material and the outward magnetic pressure. Further time evolution of these simulations will be needed to determine whether $a_{\bullet} = 0.998$ continues to have a larger variability, or if it will reach a more stable state eventually.

4.1.3. Jet Power

As discussed previously, under the Blandford-Znajek mechanism it is expected that as spin increases, so too will jet power and that the jet power output may even overcome the energy gained via accretion.

We examine this using the dimensionless jet power efficiency, η, as defined by equation 3. We compare the jet power efficiencies for both spin cases to one another and also to the analytical approximation of η as a function of spin presented in equation 4. We measure both the jet power and accretion rate, which are used to calculate jet power efficiency, at $5r_g$.
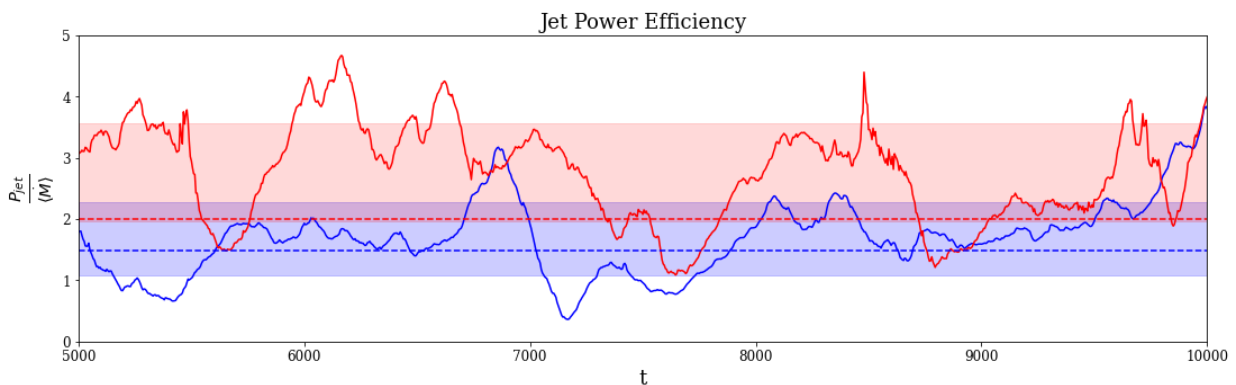
Figure 9. This plot shows the jet power efficiencies of $a_{\bullet} = 0.9375$ (blue) and $a_{\bullet} = 0.998$ (red) as a function of time. Additionally, the dashed horizontal lines reflect the predicted jet power based on equation 4 from Tcheckhovskoy et al. (2010) (Tchekhovskoy et al., 2010). The highlighted red and blue sections correspond to the mean jet power efficiency $\pm 1\sigma$ for $a_{\bullet} = 0.9375$ and 0.998 respectively.

From the graph above we find that our jet power efficiency is, on average, larger than predicted for both the $a_{\bullet} = 0.9375$ and $a_{\bullet} = 0.998$ case. In particular, for the near-maximal case, the jet power efficiency is much larger than predicted with the average efficiency being ≈ 2.766 meanwhile the predicted efficiency was only ≈ 2.0.

Upon taking time averages of jet power efficiency for both simulations, we compared our results to the proposed equation of η as a function of spin presented in Narayan et al. (2022). Narayan et al.'s setup is such that that the predicted curve is posed as some function $\eta(\phi_B)$ where ϕ_B is also a predicted magnetization curve fit to their simulations. To evaluate the influence of magnetization specifically on our results, we evaluated that same function, but with $\langle\phi_{BH}\rangle$, our observed average magnetization, as the argument instead. We denote these points as $\eta(\langle\phi_{BH}\rangle)$.
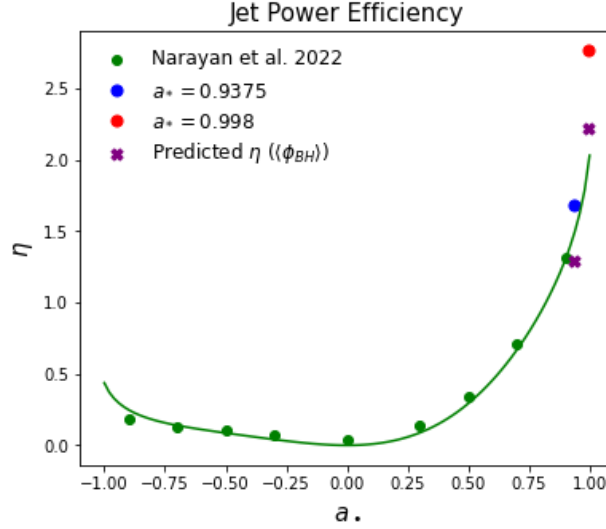
Figure 10. Above is a plot showing the jet power efficiency as a function of spin. Green indicates previously calculated values and the predicted curve (Narayan et al., 2022). The blue and red dots indicate our observed average jet power efficiency. The purple crosses indicate the predicted efficiency based on the true values for magnetization (Tchekhovskoy et al., 2010).

The average jet power efficiency for our simulations is significantly higher than predicted for the near-maximal case, and it remains higher than the $\eta(\langle\phi_{BH}\rangle)$ prediction as well. Going forward we will continue to run our GRMHD simulations for a longer period of time to see if this trend continues or if there's some other aspect that is contributing to the high efficiency.

Since the jet extracts rotational energy from the black hole, we also expect it to significantly impact the spin and we can track this impact with the spin-up parameter introduced in equation 5. Note that the spin-up values shown in the graph below were taken at $5r_g$. We approximate uncertainty for the spin-up parameter based on the equation 17, where $\dot{J}$ is the angular momentum flux and $\dot{E}$ is the energy flux which relate to s via equation 15. N is the number of samples taken, which in this case is 1,001. $\sigma_{\dot{J}}, \sigma_{\dot{E}}$, and $\sigma_{\dot{M}}$ are the standard deviations for each variable.

$$s = \frac{\dot{J}}{\dot{M}} - 2a_\bullet \frac{\dot{E}}{\dot{M}} \tag{15}$$

$$\sigma_s = \frac{1}{\sqrt{N}} \sqrt{(\frac{\partial s}{\partial \dot{J}}\sigma_{\dot{J}})^2 + (\frac{\partial s}{\partial \dot{E}}\sigma_{\dot{E}})^2 + (\frac{\partial s}{\partial \dot{M}}\sigma_{\dot{M}})^2} \tag{16}$$

$$\sigma_s = \frac{1}{\sqrt{N}} \sqrt{\left(\frac{\sigma_{\dot{J}}}{\langle\dot{M}\rangle}\right)^2 + \left[\left(\frac{\langle \dot{J}\rangle}{\langle\dot{M}\rangle^2} + \frac{2a_\bullet\langle\dot{E}\rangle}{\langle\dot{M}\rangle^2}\right)\sigma_{\dot{M}}\right]^2 + \left(\frac{2a_\bullet}{\langle\dot{M}\rangle}\sigma_{\dot{E}}\right)^2} \tag{17}$$
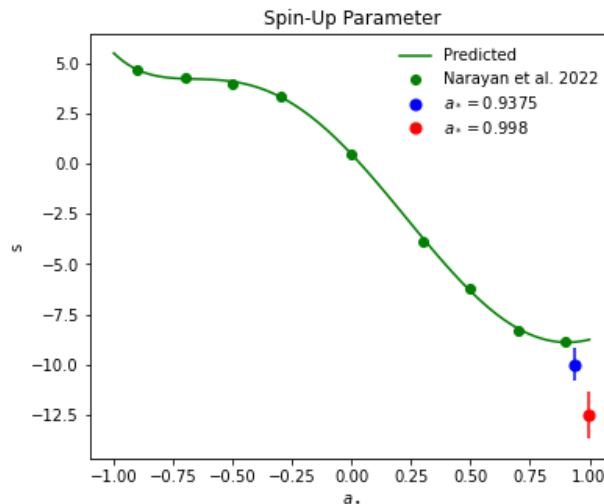
Figure 11. Above is a plot of the spin-up parameter as a function of spin. Green indicates previously calculated values and the predicted curve (Narayan et al., 2022). The blue and red dots indicate our observed average spin-up parameter. The error bars indicate $\pm 5\sigma_s$ based on our calculation of σ_s outlined above.

As seen above, the spin-up parameter is more significantly negative for the 0.9375 and 0.998 runs than predicted. This corresponds to a more intense and rapid spin-down of the black hole by its incredibly powerful jet. The error bars further indicate the significance of our results, as there is no overlap between both cases and their predicted values or between the two spin cases. The error for the near-maximal case is slightly higher than for the 0.9375 case, which is likely in part thanks to the increased variability in accretion noted before. Continuing these simulations for longer would increase sample size, further increasing our confidence in these measurements.

4.2. Observable Signatures

In order to roughly approximate the EHT's observational capabilities we apply a Gaussian blur to images produced such that they have a final resolution of 20μas. This shall be the default resolution for all figures and analysis unless otherwise specified.

Within our models, ions and electrons are not in thermal equilibrium and instead we define their temperature ratio for two regimes: 1.) the region where gas pressure dominates and 2.) the region where magnetic pressure dominates (Mościbrodzka et al., 2016). The first regime is controlled by the parameter R_{high} and the second by R_{low}. The equation for these two parameters is written below, where T_p is the ion temperature, T_e is the electron temperature, $\beta = P_{gas}/P_{mag}$, and β_{crit} is the critical pressure ratio which we take to be 1 (Mościbrodzka et al., 2016).

$$\frac{T_p}{T_e} = R_{high} \frac{(\beta^2/\beta_{crit}^2)}{1 + (\beta^2/\beta_{crit}^2)} + R_{low} \frac{1}{1 + (\beta^2/\beta_{crit}^2)} \tag{18}$$

R_{high} and R_{low} are important parameters when imaging because the temperature of ions vs electrons influences synchrotron radiation and self-absorption, which in turn significantly impacts observed flux and Faraday rotation depth (Event Horizon Telescope Collaboration et al., 2024b). For the runs discussed in this paper we use an $R_{high} = 160$ and $R_{low} = 1$, but plan to explore more values of it soon.

4.2.1. Image Differences

Using IPOLE we created movies for the $a_\bullet = 0.998$ and $a_\bullet = 0.9375$ runs over the course of $5,000 - 10,000 t_g$.

The videos aren't directly comparable frame by frame since the variability is driven by random instantiations of the turbulence. That being said we are able to evaluate trends over time by evaluating the light curve shown below.
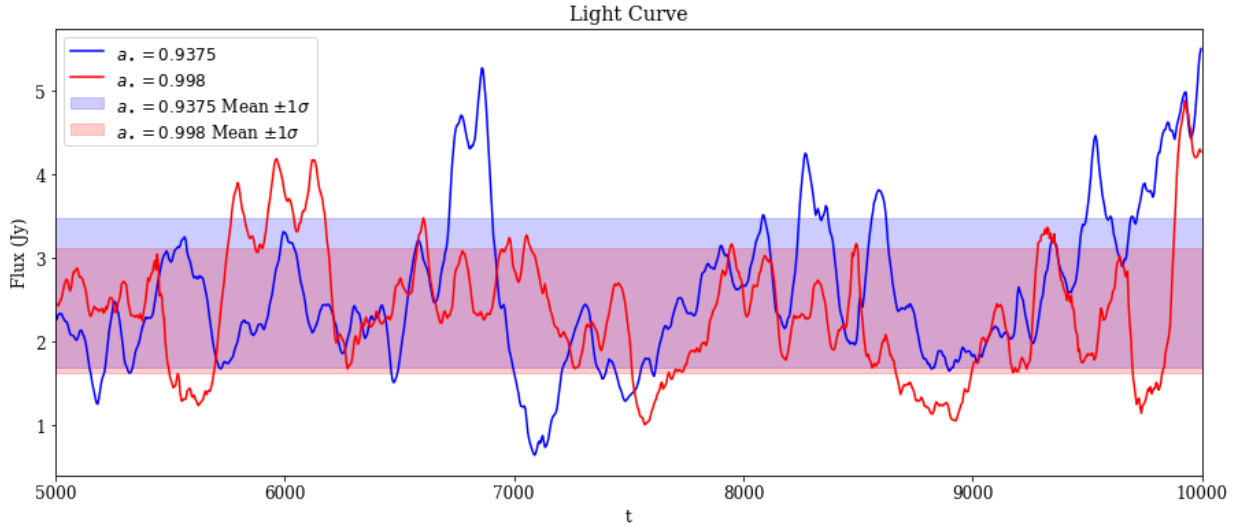
Figure 12. Above is the light curve of total flux for our $a_\bullet = 0.998$ and $a_\bullet = 0.9375$ runs.

By eye, the light curves between the two spins exhibit similar variability amplitudes and timescales. Variability is of particular importance when modeling Sgr A* because, as noted in Event Horizon Telescope Collaboration et al. (2022b), nearly all models of Sgr A* exhibit higher variability than we actually observe. Based off of our results, $a_\bullet = 0.998$ models wouldn't solve this problem, as the standard deviation only slightly decreases for our $a_\bullet = 0.998$ run (0.749 Jy) compared to our $a_\bullet = 0.9375$ run (0.894 Jy). Longer simulation timescales are needed to further understand the impact that near-maximal spin has on variability.

Aside from the light curve, we can also examine the overall image differences by taking an average over the full time span.
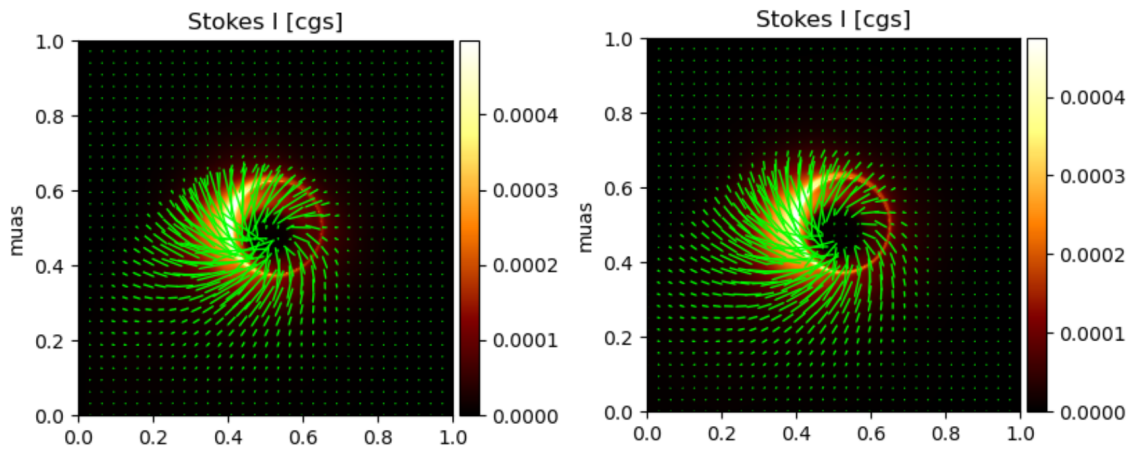
Figure 13. Above are the time averaged images for the $a_\bullet = 0.998$ (left) and $a_\bullet = 0.9375$ runs (right) for a resolution of $0.625\mu as$. The average is taken over the course of $5,000 - 10,000 t_g$ and involves averaging all stokes parameters.

The average images for the $a_\bullet = 0.9375$ and $a_\bullet = 0.998$ runs are remarkably similar, despite having giant

differences in jet power efficiency. This demonstrates the observational challenges with distinguishing even very large jet power efficiencies within EHT observations.

4.2.2. Polarization

Within the IPOLE images we are also able to examine polarization. This is a key aspect of the images as most of the emission EHT detects comes from synchrotron radiation which occurs when relativistic charged particles are rotated around magnetic field lines. The resulting radiation is polarized perpendicular to the magnetic field projected onto the sky, and so by determining linear polarization you can probe the magnetic field structure of a black hole.

Below is a list of the most relevant polarization metrics, which are described in more detail below.

- m_{net}
- v_{net}
- Phase and magnitude of β_2

4.2.2.1. m_{net} The spatially unresolved linear polarization fraction, obtainable by e.g., a single-dish measurement of a source. This is calculated via.

$$m_{net} = \frac{\sqrt{(\Sigma_{pixel}Q)^2 + (\Sigma_{pixel}U)^2}}{\Sigma_{pixel}I} \tag{19}$$

where $I, Q,$ and U are the Stokes parameters.

4.2.2.2. v_{net} The analogous quantity for circular polarization, calculated via

$$v_{net} = \frac{\Sigma_{pixel}V}{\Sigma_{pixel}I} \tag{20}$$

Small amounts of circular polarization naturally occur as part of synchrotron radiation, however the primary source of circular polarization within EHT images would be due to Faraday conversion (Ricarte et al., 2021; Event Horizon Telescope Collaboration et al., 2023). Essentially, as linearly polarized light propagates along its wavevector, one of two mechanisms convert Q to U which then can be Faraday converted into circular polarization (Ricarte et al., 2021).

v_{net} specifically helps inform the direction of the poloidal field in the observer's line of sight (Event Horizon Telescope Collaboration et al., 2024b).

4.2.2.3. β_2 The 2nd mode decomposition coefficient defined by the equation below (Palumbo et al., 2020).

$$\beta_2 = \frac{1}{I_{ann}} \int_{\rho_{min}}^{\rho_{max}} \int_0^{2\pi} P(\rho, \varphi) e^{-i2\varphi} \rho \, d\varphi \, d\rho \tag{21}$$

where I_{ann} is the total Stokes I flux in the annulus, ρ_{min} and ρ_{max} are the radial extent of the annulus, and $P(\rho, \varphi)$ is the complex valued polarization field $Q(\rho, \varphi) + iU(\rho, \varphi)$.

In a simpler sense, β_2 is a complex number that summarizes the rotationally-symmetric structure of linear polarization ticks. The phase encodes the pitch angle, while the magnitude encodes the strength of this mode(Palumbo et al., 2020). This can be best visualized with figure 14 below from Figure 1 in Palumbo et al. (2020) (Palumbo et al., 2020).

Because the underlying magnetic field structure is rotationally symmetric, numerous studies have demonstrated that β_2 is a sensitive tracer of spin (Palumbo et al., 2020; Emami et al., 2023; Qiu et al., 2023; Chael et al., 2023). Thus, it is of interest how rapidly this observable changes between our two spin values.
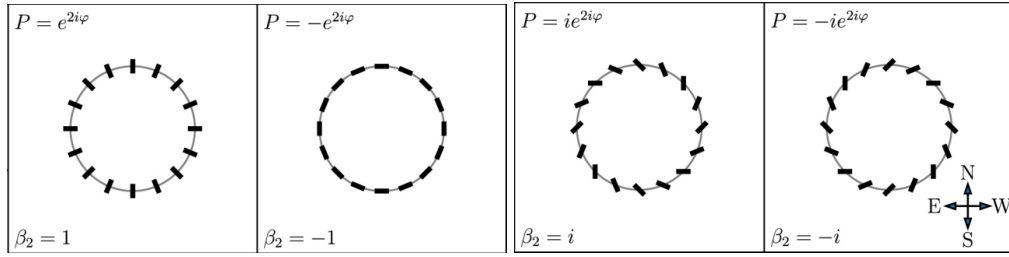
Figure 14. An illustration of polarization ticks and the corresponding β modes 1-4 from Palumbo et al. (2020), along with an depiction of polarization ticks and the corresponding phases for β_2 (Palumbo et al., 2020).
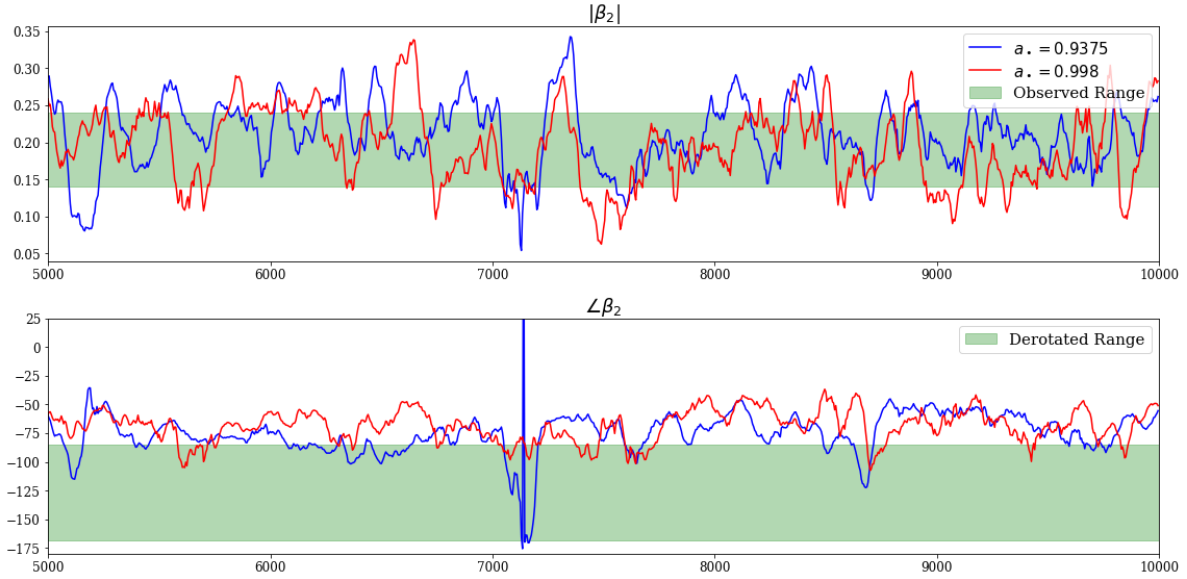
Figure 15. Above are 2 plots showing the magnitude and argument of β_2. The blue indicates our $a_\bullet = 0.9375$ run while red indicates the 0.998 run. The green shows the observationally constrained values for Sgr A* according to the EHT (Event Horizon Telescope Collaboration et al., 2024b).
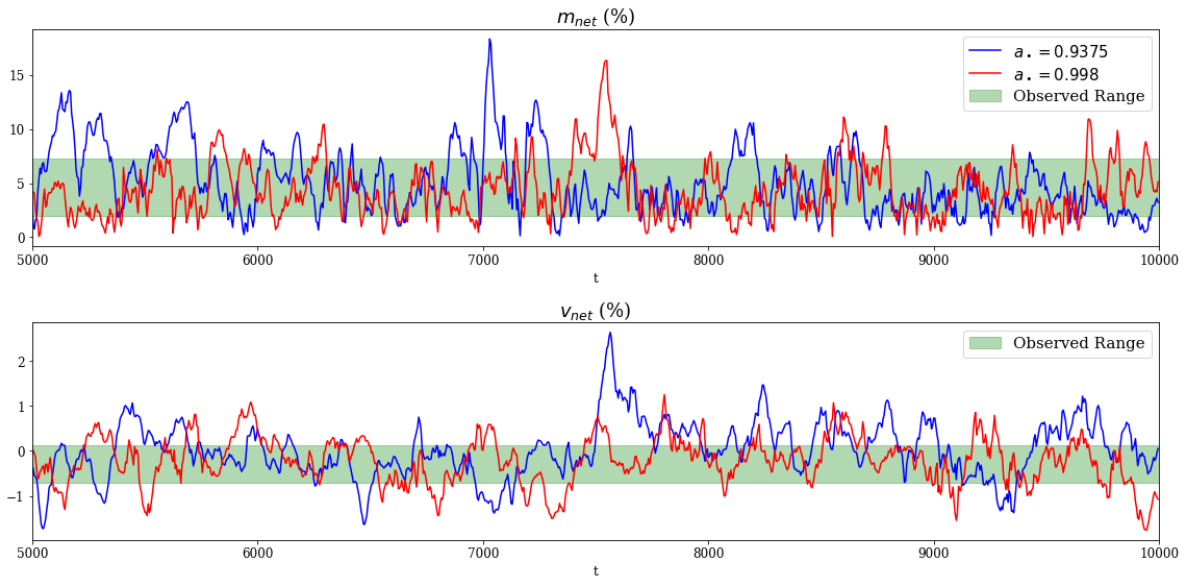
Figure 16. Above are 2 plots showing the linear (m_{net}) and circular (v_{net}) polarization fraction. The blue indicates our $a_\bullet = 0.9375$ run while red indicates the 0.998 run. The green shows the observationally constrained values for Sgr A* according to the EHT (Event Horizon Telescope Collaboration et al., 2024b).

4.2.2.4. Polarimetric Results Above we note very similar values for almost all of our polarimetric quantities between the 0.998 and 0.9375 simulations. Both spin values seem to fit well with Sgr A* constraints for all metrics, although the agreement with $\angle\beta_2$ is marginal. This is fully consistent with previous studies (Event Horizon Telescope Collaboration et al., 2024b). We report no significant difference in these polarized metrics between $a_\bullet = 0.9375$ and $a_\bullet = 0.998$, suggesting that EHT observations of Sgr A* are at present consistent with a $a_\bullet = 0.998$ black hole.

4.2.3. n=1 Photon Ring

One of the key scientific goals of ngEHT alongside BHEX is to resolve the n=1 photon ring (Johnson et al., 2024). For that reason, it's important to check the observability in differences of the photon ring between $a_\bullet = 0.998$ and $a_\bullet = 0.9375$.

As seen in figure 2, the most intense effects to the critical curve, and therefore the photon ring, occurs when the black hole is viewed at an inclination of 90 °. For this reason, we image the $a_\bullet = 0.998$ and 0.9375 photon rings at an inclination of 90 °.

The manner in which IPOLE isolates photon rings is such that, at 90 °, photons which have only completed approximately a half-orbit are included in the n=1 ring image. These photons don't actually belong in the n=1 image, but instead in the n=0 image as they haven't completed a full orbit. Because of this subtlety within IPOLE, our images technically include what IPOLE considers to be the n=2 photon ring. This better reflects the true n=1 photon ring image as all of the photons included have compelted at least one orbit around the black hole. For simplicity's sake, we will refer to this simply as the n=1 photon ring.

The image below was produced by imaging the n=1 photon ring for a snapshot for both the $a_\bullet = 0.998$ and 0.9375 simulation and overlaying the two images in order to highlight their differences.
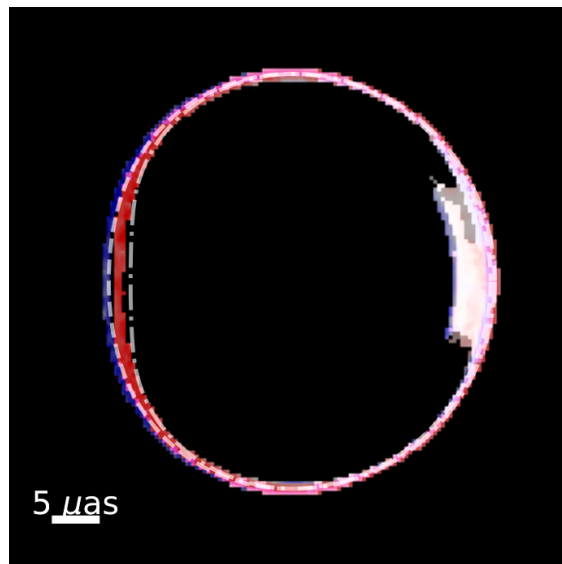
Figure 17. Overlapped IPOLE images of the n=1 photon ring taken with a resolution of 0.5μas for the $a_\bullet = 0.9375$ (blue) and $a_\bullet = 0.998$ (red) case. The dashed lines correlate to the n=∞ rings for $a_\bullet = 0.9375$ (white dashed curve) and $a_\bullet = 0.998$ (white dashed and dotted curve).

As seen in figure 17, there's a visible distortion of the photon ring for the $a_\bullet = 0.998$ case. This distortion is subtle and is approximately of order of a few μas, so further work will be need to be done to determine if it would be resolvable with future ngEHT and BHEX resolution.

Additionally, the distortion within our IPOLE images is only slightly less prominent than the expected distortion of the n=∞ ring. This is consistent with theoretical expectations since the $n = 1$ ring is not entirely insensitive to the $n = 0$ emission profile. However, it's important to note that as n increases the corresponding rings become exponentially fainter. Only the $n = 1$ will resolvable using BHEX, with $n > 1$ requiring telescopes as distant as the moon (Johnson et al., 2020). Having access to only $n = 1$, we have demonstrated that fitting this curve with an $n = \infty$ template would lead to an under-estimate of the spin.

5. CONCLUSION

In summary, we have found that

1. $a_\bullet = 0.998$ models show similar accretion rates & magnetization as their $a_\bullet = 0.9375$ counterparts

2. Jet efficiency increases more than expected for $a_\bullet = 0.998$, and spin-up also deviates from previous predictions.

3. The observable polarimetric quantities of $a_\bullet = 0.998$ and 0.9375 models are very similar, and roughly agree with current Sgr A* EHT observations.

4. At high resolution, near-maximal spin results in a visible distortion of the photon ring image.

So far, both the $a_\bullet = 0.998$ and $a_\bullet = 0.9375$ simulations match existing constraints on Sgr A*, but additional constraints will be considered in the future, including time variability. In our results so far, the jet efficiency is the most promising way to discriminate between these two spin values, although this is difficult to access observationally.

As extensions to the EHT are developed both on land, with the next-generation EHT project, and in space, with the Black Hole Explorer mission, signatures of near-maximal spin may become observationally accessible via the photon ring.

Our results regarding the spin-up parameter and jet power efficiency would suggest faster than expected spin-down of SMBHs over cosmological timescales. Depending on accretion rate, this could significantly influence AGN feedback and could help us better model galaxy evolution.

One main limitation of our research so far is that we have only run simulations out to $10,000t_g$, in comparison to the $100,000t_g$ used in similar papers (Narayan et al., 2022). Going forward, we plan on extending our simulations, which will help ensure greater confidence in the stability and significance of our results. Additionally, this will allow us to better compare model variability to Sgr A*.

ACKNOWLEDGEMENTS

References

Event Horizon Telescope Collaboration et al. First M87 Event Horizon Telescope Results. I. The Shadow of the Supermassive Black Hole. *ApJ*, 875(1):L1, April 2019a. doi:10.3847/2041-8213/ab0ec7.

Event Horizon Telescope Collaboration et al. First Sagittarius A* Event Horizon Telescope Results. I. The Shadow of the Supermassive Black Hole in the Center of the Milky Way. *ApJ*, 930(2):L12, May 2022a. doi:10.3847/2041-8213/ac6674.

Event Horizon Telescope Collaboration et al. First Sagittarius A* Event Horizon Telescope Results. VII. Polarization of the Ring. *ApJ*, 964(2):L25, April 2024a. doi:10.3847/2041-8213/ad2df0.

Event Horizon Telescope Collaboration et al. First M87 Event Horizon Telescope Results. VII. Polarization of the Ring. *ApJ*, 910(1):L12, March 2021. doi:10.3847/2041-8213/abe71d.

Michael D. Johnson, Kazunori Akiyama, Lindy Blackburn, Katherine L. Bouman, Avery E. Broderick, Vitor Cardoso, Rob P. Fender, Christian M. Fromm, Peter Galison, José L. Gómez, Daryl Haggard, Matthew L. Lister, Andrei P. Lobanov, Sera Markoff, Ramesh Narayan, Priyamvada Natarajan, Tiffany Nichols, Dominic W. Pesce, Ziri Younsi, Andrew Chael, Koushik Chatterjee, Ryan Chaves, Juliusz Doboszewski, Richard Dodson, Sheperd S. Doeleman, Jamee Elder, Garret Fitzpatrick, Kari Haworth, Janice Houston, Sara Issaoun, Yuri Y. Kovalev, Aviad Levis, Rocco Lico, Alexandru Marcoci, Niels C. M. Martens, Neil M. Nagar, Aaron Oppenheimer, Daniel C. M. Palumbo, Angelo Ricarte, María J. Rioja, Freek Roelofs, Ann C. Thresher, Paul Tiede, Jonathan Weintroub, and Maciek Wielgus. Key Science Goals for the Next-Generation Event Horizon Telescope. *Galaxies*, 11(3):61, April 2023. doi:10.3390/galaxies11030061.

Michael Johnson, Kazunori Akiyama, Rebecca Baturin, Bryan Bilyeu, Lindy Blackburn, Don Boroson, Alejandro Cárdenas-Avendaño, Andrew Chael, Chi-kwan Chan, Dominic Chang, Peter Cheimets, Cathy Chou, Sheperd S. Doeleman, Joseph Farah, Peter Galison, Ronald S. Gamble, Charles F. Gammie, Zachary Gelles, José L. Gómez, Samuel E. Gralla, Paul K. Grimes, Leonid I. Gurvits, Shahar Hadar, Kari Haworth, Kazuhiro Hada, Michael H. Hecht, Mareki Honma, Janice Houston, Ben Hudson, Sara Issaoun, He Jia, Svetlana Jorstad, Jens Kauffman, Yuri Kovalev, Peter Kurczynski, Robert Lafon, Alexandru Lupsasca, Robert Lehmensiek, Chung-Pei Ma, Daniel P. Marrone, Alan P. Marscher, Gary Melnick, Ramesh Narayan, Kotaro Niinuma, Scott C. Noble, Eric J. Palmer, Daniel C. M. Palumbo, Lenny Paritsky, Eliad Peretz, Dominic Pesce, Alexander Plavin, Eliot Quataert, Hannah Rana, Angelo Ricarte, Freek Roelofs, Katia Shtyrkova, Laura C. Sinclair, Jeffrey Small, Tirupati Kumara Sridharan, Ranjani Srinivasan, Andrew Strominger, Paul Tiede, Edward Tong, Jade Wang, Jonathan Weintroub, Maciek Wielgus, and George N. Wong. The black hole explorer: motivation and vision. In Laura E. Coyle, Marshall D. Perrin, and Shuji Matsuura, editors, *Space Telescopes and Instrumentation 2024: Optical, Infrared, and Millimeter Wave*, page 90. SPIE, August 2024. doi:10.1117/12.3019835. URL http://dx.doi.org/10.1117/12.3019835.

Event Horizon Telescope Collaboration et al. First M87 Event Horizon Telescope Results. V. Physical Origin of the Asymmetric Ring. *ApJ*, 875(1):L5, April 2019b. doi:10.3847/2041-8213/ab0f43.

Kip S. Thorne. Disk-Accretion onto a Black Hole. II. Evolution of the Hole. *ApJ*, 191:507–520, July 1974. doi:10.1086/152991.

Charles F. Gammie, Stuart L. Shapiro, and Jonathan C. McKinney. Black Hole Spin Evolution. *ApJ*, 602 (1):312–319, February 2004. doi:10.1086/380996.

Stuart L. Shapiro. Spin, Accretion, and the Cosmological Growth of Supermassive Black Holes. *ApJ*, 620 (1):59–68, February 2005. doi:10.1086/427065.

Ramesh Narayan, Andrew Chael, Koushik Chatterjee, Angelo Ricarte, and Brandon Curd. Jets in magnetically arrested hot accretion flows: geometry, power, and black hole spin-down. *MNRAS*, 511(3): 3795–3813, April 2022. doi:10.1093/mnras/stac285.

Angelo Ricarte, Ramesh Narayan, and Brandon Curd. Recipes for Jet Feedback and Spin Evolution of Black Holes with Strongly Magnetized Super-Eddington Accretion Disks. *ApJ*, 954(1):L22, September 2023a. doi:10.3847/2041-8213/aceda5.

Beverly Lowell, Jonatan Jacquemin-Ide, Alexander Tchekhovskoy, and Alex Duncan. Rapid Black Hole Spin-down by Thick Magnetically Arrested Disks. *ApJ*, 960(1):82, January 2024. doi:10.3847/1538-4357/ad09af.

Beverly Lowell, Jonatan Jacquemin-Ide, Matthew Liska, and Alexander Tchekhovskoy. Evidence for Low Universal Equilibrium Black Hole Spin in Luminous Magnetically Arrested Disks. *arXiv e-prints*, art. arXiv:2502.17559, February 2025. doi:10.48550/arXiv.2502.17559.

Emanuele Berti and Marta Volonteri. Cosmological Black Hole Spin Evolution by Mergers and Accretion. *ApJ*, 684(2):822–828, September 2008. doi:10.1086/590379.

Angelo Ricarte, Priyamvada Natarajan, Ramesh Narayan, and Daniel C. M. Palumbo. Multimessenger Probes of Supermassive Black Hole Spin Evolution. *ApJ*, 980(1):136, February 2025. doi:10.3847/1538-4357/ad9ea9.

R. D. Blandford and R. L. Znajek. Electromagnetic extraction of energy from Kerr black holes. *MNRAS*, 179:433–456, May 1977. doi:10.1093/mnras/179.3.433.

Shane W. Davis and Alexander Tchekhovskoy. Magnetohydrodynamics simulations of active galactic nucleus disks and jets. *Annual Review of Astronomy and Astrophysics*, 58(1):407–439, August 2020. ISSN 1545-4282. doi:10.1146/annurev-astro-081817-051905. URL http://dx.doi.org/10.1146/annurev-astro-081817-051905.

Alexander Tchekhovskoy, Ramesh Narayan, and Jonathan C. McKinney. Black Hole Spin and The Radio Loud/Quiet Dichotomy of Active Galactic Nuclei. *ApJ*, 711(1):50–63, March 2010. doi:10.1088/0004-637X/711/1/50.

Event Horizon Telescope Collaboration et al. First Sagittarius A* Event Horizon Telescope Results. V. Testing Astrophysical Models of the Galactic Center Black Hole. *ApJ*, 930(2):L16, May 2022b. doi:10.3847/2041-8213/ac6672.

Angelo Ricarte, Daniel C. M. Palumbo, Ramesh Narayan, Freek Roelofs, and Razieh Emami. Observational Signatures of Frame Dragging in Strong Gravity. *ApJ*, 941(1):L12, December 2022. doi:10.3847/2041-8213/aca087.

Daniel C. M. Palumbo, George N. Wong, Andrew Chael, and Michael D. Johnson. Demonstrating Photon Ring Existence with Single-baseline Polarimetry. *ApJ*, 952(2):L31, August 2023. doi:10.3847/2041-8213/ace630.

Angelo Ricarte, Paul Tiede, Razieh Emami, Aditya Tamar, and Priyamvada Natarajan. The ngEHT's Role in Measuring Supermassive Black Hole Spins. *Galaxies*, 11(1):6, January 2023b. doi:10.3390/galaxies11010006.

Andrew Chael, Michael D. Johnson, and Alexandru Lupsasca. Observing the Inner Shadow of a Black Hole:

A Direct View of the Event Horizon. *ApJ*, 918(1):6, September 2021. doi:10.3847/1538-4357/ac09ee.

Andrew Chael, Michael Johnson, and Alexandru Lupsasca. The Inner Shadow of the Black Hole in M87*: A Direct View of the Event Horizon. In *American Astronomical Society Meeting #240*, volume 240 of *American Astronomical Society Meeting Abstracts*, page 432.08, June 2022.

George N. Wong, Ben S. Prather, Vedant Dhruv, Benjamin R. Ryan, Monika Mościbrodzka, Chi-kwan Chan, Abhishek V. Joshi, Ricardo Yarza, Angelo Ricarte, Hotaka Shiokawa, Joshua C. Dolence, Scott C. Noble, Jonathan C. McKinney, and Charles F. Gammie. PATOKA: Simulating Electromagnetic Observables of Black Hole Accretion. *ApJS*, 259(2):64, April 2022. doi:10.3847/1538-4365/ac582e.

L. G. Fishbone and V. Moncrief. Relativistic fluid disks in orbit around Kerr black holes. *ApJ*, 207:962–976, August 1976. doi:10.1086/154565.

A. Mignone and Jonathan C. McKinney. Equation of state in relativistic magnetohydrodynamics: variable versus constant adiabatic index. *MNRAS*, 378(3):1118–1130, July 2007. doi:10.1111/j.1365-2966.2007.11849.x.

Ramesh Narayan, Igor V. Igumenshchev, and Marek A. Abramowicz. Magnetically Arrested Disk: an Energetically Efficient Accretion Flow. *PASJ*, 55:L69–L72, December 2003. doi:10.1093/pasj/55.6.L69.

Ramesh Narayan, Aleksander SÄ dowski, Robert F. Penna, and Akshay K. Kulkarni. GRMHD simulations of magnetized advection-dominated accretion on a non-spinning black hole: role of outflows. *MNRAS*, 426(4):3241–3259, November 2012. doi:10.1111/j.1365-2966.2012.22002.x.

M. Mościbrodzka and C. F. Gammie. IPOLE - semi-analytic scheme for relativistic polarized radiative transport. *MNRAS*, 475(1):43–54, March 2018. doi:10.1093/mnras/stx3162.

Alexander Tchekhovskoy, Ramesh Narayan, and Jonathan C. McKinney. Efficient generation of jets from magnetically arrested accretion on a rapidly spinning black hole. *MNRAS*, 418(1):L79–L83, November 2011. doi:10.1111/j.1745-3933.2011.01147.x.

A Tchekhovskoy, JC McKinney, and R Narayan. Journal of physics conference series, 2012.

Monika Mościbrodzka, Heino Falcke, and Hotaka Shiokawa. General relativistic magnetohydrodynamical simulations of the jet in M 87. *A&A*, 586:A38, February 2016. doi:10.1051/0004-6361/201526630.

Event Horizon Telescope Collaboration et al. First Sagittarius A* Event Horizon Telescope Results. VIII. Physical Interpretation of the Polarized Ring. *ApJ*, 964(2):L26, April 2024b. doi:10.3847/2041-8213/ad2df1.

Angelo Ricarte, Richard Qiu, and Ramesh Narayan. Black hole magnetic fields and their imprint on circular polarization images. *MNRAS*, 505(1):523–539, July 2021. doi:10.1093/mnras/stab1289.

Event Horizon Telescope Collaboration et al. First M87 Event Horizon Telescope Results. IX. Detection of Near-horizon Circular Polarization. *ApJ*, 957(2):L20, November 2023. doi:10.3847/2041-8213/acff70.

Daniel C. M. Palumbo, George N. Wong, and Ben S. Prather. Discriminating Accretion States via Rotational Symmetry in Simulated Polarimetric Images of M87. *ApJ*, 894(2):156, May 2020. doi:10.3847/1538-4357/ab86ac.

Razieh Emami, Angelo Ricarte, George N. Wong, Daniel Palumbo, Dominic Chang, Sheperd S. Doeleman, Avery E. Broderick, Ramesh Narayan, Maciek Wielgus, Lindy Blackburn, Ben S. Prather, Andrew A. Chael, Richard Anantua, Koushik Chatterjee, Ivan Marti-Vidal, Jose L. Gómez, Kazunori Akiyama, Matthew Liska, Lars Hernquist, Grant Tremblay, Mark Vogelsberger, Charles Alcock, Randall Smith, James Steiner, Paul Tiede, and Freek Roelofs. Unraveling Twisty Linear Polarization Morphologies in

Black Hole Images. *ApJ*, 950(1):38, June 2023. doi:10.3847/1538-4357/acc8cd.

Richard Qiu, Angelo Ricarte, Ramesh Narayan, George N. Wong, Andrew Chael, and Daniel Palumbo. Using Machine Learning to link black hole accretion flows with spatially resolved polarimetric observables. *MNRAS*, 520(4):4867–4888, April 2023. doi:10.1093/mnras/stad466.

Andrew Chael, Alexandru Lupsasca, George N. Wong, and Eliot Quataert. Black Hole Polarimetry I. A Signature of Electromagnetic Energy Extraction. *ApJ*, 958(1):65, November 2023. doi:10.3847/1538-4357/acf92d.

Michael D. Johnson, Alexandru Lupsasca, Andrew Strominger, George N. Wong, Shahar Hadar, Daniel Kapec, Ramesh Narayan, Andrew Chael, Charles F. Gammie, Peter Galison, Daniel C. M. Palumbo, Sheperd S. Doeleman, Lindy Blackburn, Maciek Wielgus, Dominic W. Pesce, Joseph R. Farah, and James M. Moran. Universal interferometric signatures of a black hole's photon ring. *Science Advances*, 6(12):eaaz1310, March 2020. doi:10.1126/sciadv.aaz1310.

This paper has been typeset from a TEX / LATEX file prepared by the author.